


☐

I'm not robot

  
reCAPTCHA

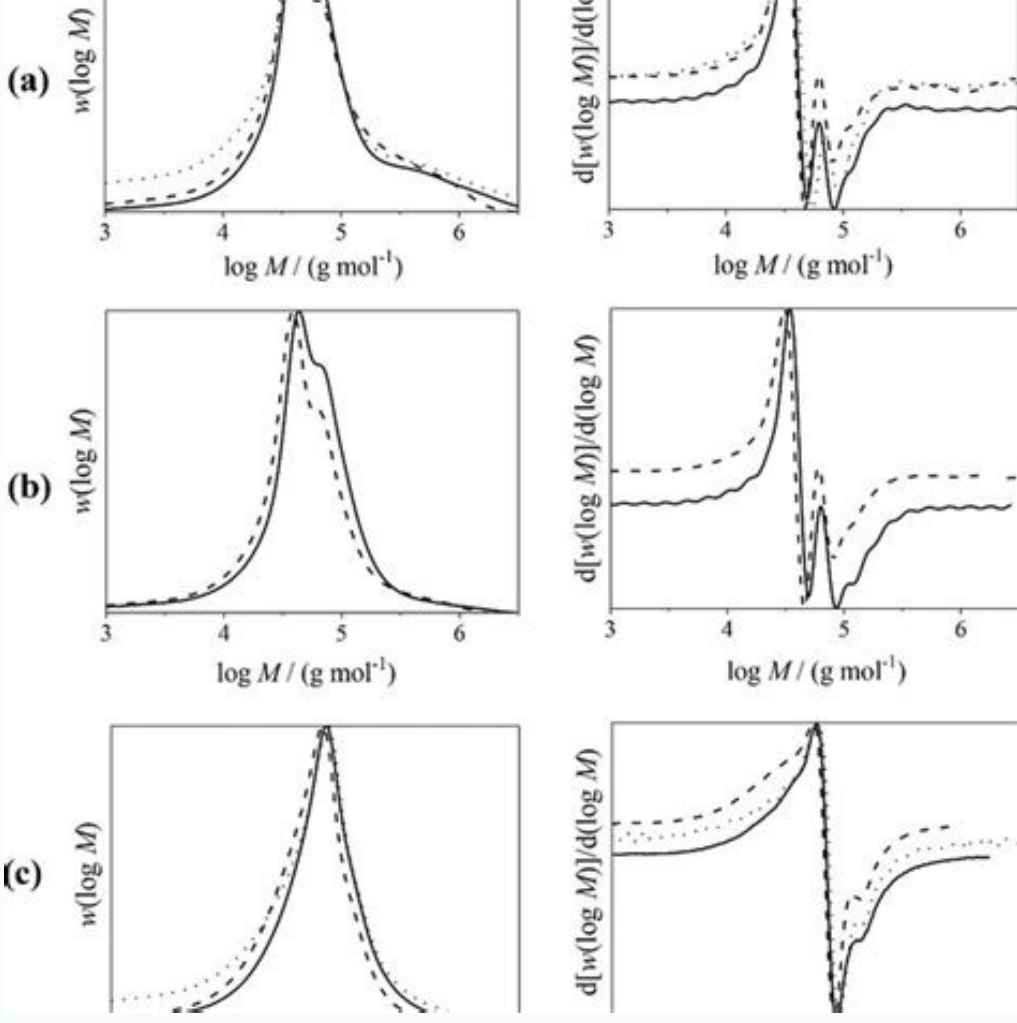
I'm not robot!

## Poly methacrylic acid glass transition temperature

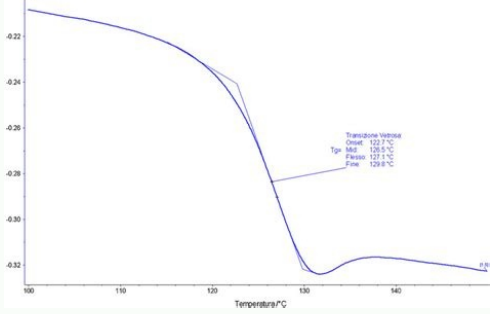
**What is glass transition temperature of polymers. Polymers with high glass transition temperature. Melting point vs glass transition. Ceramic glass transition temperature. Poly(methacrylic acid) glass transition temperature.**

Access through your institutionVolume 504, 15 October 2017, Pages 758-764 rights and contentIt is common for a polymer surface to shift towards the thermodynamic equilibrium state by minimizing its surface free energy via segregating the low surface energy components, especially when the polymer chains are free to move. For example, Akhter et al. [1] showed in their angle-resolved X-ray photoelectron spectroscopy (XPS) data that more than 75% of the phenyl groups of polystyrene (PS) films were orientated away from the bulk and the concentration of the phenyl groups at the top-most surface decreased after annealing at 150 °C.

[2] demonstrated that the contact angle of deionized water on annealed films of poly(methyl methacrylate) (PMMA) increased with temperature, even if the temperatures tested were below its bulk glass transition temperature (Tg). The surface chain conformation of PMMA has also been extensively studied by surface-sensitive techniques, such as sum-frequency-generation (SFG) spectroscopy [2], [3], [4], [5], [6]. However, different research groups have come up with rather conflicting interpretations of the SFG results on the surface conformation of PMMA. For instance, Tateishi et al. [3] compared the SFG spectra of unannealed and annealed PMMA films, and concluded that the annealed ones had more ordered methylene groups at the surface, while Wang et al. [5] Kweskin et al. [7] and Li et al. [8] found that the symmetrical stretching of the OCH3 component of the ester side chain dominated in the SFG spectrum of annealed PMMA films for the ssp polarization combination. The conformation of PMMA was not clearly elucidated until recently, when Zhu et al. [4] and Jha et al. [9] produced more definitive results using both SFG spectroscopy and molecular dynamics (MD) simulation. Generally, they concluded that the ester methyl groups were more ordered than the methylene groups and the ester methyl groups were in excess at the surface of isotactic PMMA. Also, they commented that it was difficult to determine the exact orientation of different chemical groups of PMMA at the surface from the SFG spectroscopic results alone because the hydrocarbon peaks overlapped in the wavenumber range of 2800–3100 cm<sup>−1</sup> in the SFG spectra. And although SFG spectroscopy is one of the most surface-sensitive techniques, the bulk contribution is not completely negligible [10]. Time-of-flight secondary ion mass spectrometry (ToF-SIMS) could be a better technique for determining the surface conformation of PMMA due to its high surface sensitivity and extremely high mass resolution [11], [12], [13], [14], [15], [16]. Furthermore, the origin of different positive and negative ion fragments from PMMAs with varied tacticity and chemical derivatization has been studied extensively in terms of their chain-breaking mechanisms and degradation pathways under primary ion bombardment thus revealing different surface compositions [17], [18], [19], [20], [21], [22]. It is likely that a detailed analysis of ToF-SIMS spectra will produce results that are more definitive.In our previous studies on PS [11] and poly(2, 3, 4, 5, 6-pentafluorostyrene) (5FPS) [12], ToF-SIMS spectra obtained at various temperatures indicated that the surface conformation of these polymers changed after annealing at temperatures higher than their corresponding surface transition temperatures (TT s) which are suspected to be related to their surface glass transition temperatures (TgS s). The concentration of the phenyl groups of a spin-coated PS film was shown to decrease after the film was annealed at a temperature above its TT because the surface energy of its phenyl groups is higher than that of its hydrocarbon backbone. On the contrary, the concentration of the fluorinated phenyl groups of a 5FPS spin-coated film was found to increase after it was annealed at a temperature above its TT because the surface energy of the fluorinated phenyl groups is lower than that of the hydrocarbon backbone of 5FPS. Interestingly, the results of contact angle measurements also indicated that this kind of re-orientation of the chemical groups in PS and 5FPS occurred approximately at their TT s. In the literature, very few attempts have been made to determine TgS by probing the surface structure of PMMA as a function of temperature. To the best of our knowledge, only Li et al. [8] with the use of SFG spectroscopy, detected a transition temperature of 67 °C, at which the PMMA chains near the surface were fully relaxed. However, as mentioned above, due to the limitations of SFG spectroscopy, they were unable to provide detailed information on the structure of the PMMA surface.In this work, we determined the TT of PMMA as a function of molecular weight using ToF-SIMS and principal component analysis (PCA) as well as contact angle measurements.A series of monodisperse PMMAs with weight-average molecular weights of 6000, 125,000 and 350,000 g/mole denoted by PMMA-6k, PMMA-125k and PMMA-350k, respectively, were purchased from Polysciences, Inc. (Warrington, Pennsylvania), while PMMA-48k with a molecular weight of 48,000 g/mole was purchased from Polymer Source, Inc. (Montreal, Quebec). Toluene (from Acros Organics) of reagent grade was used without further purification. Table 1 summarizes the molecular weights and the Tg s of the PMMAs.Fig. 1 shows a positive ion spectrum of PMMA-48k at room temperature. PCA of ToF-SIMS positive ion spectra of the unannealed PMMA films and films annealed at different temperatures was conducted. All the peaks in the ToF-SIMS spectra were included in the PCA calculation. Fig. 2, Fig. 3, Fig. 4 shows the PCA scores plots and the corresponding loadings plots of the positive ions of 200-nm-thick PMMA-6k, PMMA-48k, and PMMA-350k, respectively. In the PCA scores plot of a 200-nm-thick PMMA-6k filmPCA of ToF-SIMS spectra and contact angle measurements of unannealed and annealed films revealed that the TT of PMMA is about 50 to 60 °C below its bulk Tg. When the annealing temperature is above TT, the PMMA chains re-orientate by turning the ester groups towards the surface so that more methoxy groups end up at the topmost surface. This change in the top-most surface chemical composition at the TT were detected by ToF-SIMS and contact angle measurements.

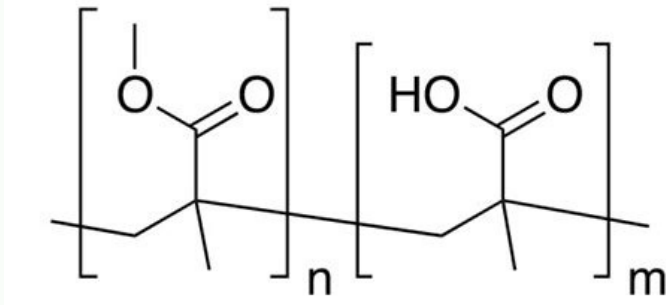


The TT s of PMMA, PS [11] and 5FPS [12]The work described in this paper was fully supported by the Research Grants Council of the Hong Kong Special Administrative Region, China (Grant no. 600513).S. Akhter et al.Y. Fu et al.Y.T.R. Lau et al.A. Horinouchi et al.Y. Tateishi et al.H. Zhu et al.J. Wang et al.J. Xu et al.S.J. Kweskin et al.Q. Li et al.K.C. Jha et al.H. Held et al.Y. Fu et al.S. Affrossman et al.X. Vanden Eynde et al.Surface and thin films are important in modern technologies and there is growing demand for their characterization. Secondary ion mass spectrometry (SIMS) is universally used for extracting information on the chemical composition of surfaces. This study shows that it can provide information about the physical (mechanical) properties of thermoset polymer surfaces. The intensities of backscattered Arn<sup>+</sup> clusters were measured upon 10 keV Ar3000<sup>+</sup> gas cluster ion bombardment of polymer films. Tyrosol diaminodiphenylmethane based benzoxazine thermosets with different curing cycles were used. The intensity ratios Ar2<sup>+</sup>/(Ar2<sup>+</sup>+Ar3<sup>+</sup>) and Ar2<sup>+</sup>/(Ar2<sup>+</sup>+Ar4<sup>+</sup>) were highly sensitive to the physical changes of the thermoset coating surfaces as a function of their curing cycle and of temperature. These intensity ratios provide direct access to the surface transition temperature TT (related to the bulk glass transition Tg), and show a dependence on the curing degree below and above TT. Moreover, we discuss the influence of surface contamination and clusters induced roughness on the measured values. Our results suggest that contamination has a dramatic influence on the intensity of backscattered Arn<sup>+</sup> clusters, while that of roughness appears to be minor.



This study constitutes a step forward towards a quantitative assessment of the mechanical properties of polymer coating surfaces using SIMS.Lignocellulosic fiber, composed of hydrophilic component (carbohydrates, including cellulose and hemicellulose) and hydrophobic component (lignin), is widely used in bio-composites, paper and paperboard products, and other fiber-based bio-products. The surface wettability of cylinder-shaped fibers, focusing on the liquid spreading ability on fiber surface, essentially has an important effect on many kinds of fiber properties. A novel measurement of contact angle (“liquid-bridge” testing) was utilized for the calculation of surface free energy, expressed as the evaluation of fiber surface wettability. The results showed that the fiber contact angle determined by the “liquid-bridge” testing was quite similar to that measured by the traditional sessile drop technique. The fiber surface free energy increased dramatically from 46.63 mJ m<sup>−2</sup> to 54.45 mJ m<sup>−2</sup>, calculated by the fiber contact angle with water (74.30° to 43.24°) and glycerol (64.50° to 49.41°), when the PFT mechanical treatment was strengthened up to 15,000 rev. This novel method has also been applied to test the positive variation and sensitivity of surface wettability with the increase of fiber surface roughness and surface pore size.View all citing articles on ScopusA spherical titanium dioxide/silver (TiO2/Ag) composite and a flower-like hierarchical TiO2/Ag composite were prepared via a template-induced method and a solvothermal method based on the Ag/Carbon spheres templates followed by calcination treatment, respectively. The morphologies of the composites were controlled by changing the concentration of reactants and calcination temperature. The antibacterial efficiency of the composites was evaluated with both Gram-negative Escherichia coli and Gram-positive Staphylococcus aureus, respectively. The minimal inhibitory concentration, morphological evolution of bacteria and fluorescent-based cell wall/membrane integrity were assayed. The synergistic effects of reactive oxygen species (ROS) and silver ions were observed, which lead to superior antibacterial activities of these TiO2/Ag composites with a bacteriostatic rate as high as 99% even in the absence of light. The morphological effect of the composites on the antibacterial efficacy was also investigated. In addition, a durable antimicrobial coating was also fabricated by incorporating the hierarchical TiO2/Ag composite into a commercial emulsion solution of polyvinyl acetate, which exhibited a promising application in bacterial sensitive locations.A series of magnetic recyclable bismuth oxydide (BiOI)/polyacrylic anion exchange resin (PAER) composites with visible light responses have been synthesized for the first time through a facile and low-cost method at normal temperature. The photocatalytic performances of BiOI/PAER composites were evaluated by photodegrading 1-amino-8-naphthol-3,6-disulfonic acid under visible light. It was found that 1-amino-8-naphthol-3,6-disulfonic acid removal rate reached to 90.1% (BiOI/PAER-2), which was higher than the pure BiOI (50.3%) in 60 min. The enhanced photocatalytic performance of BiOI/PAER composites should be attributed to the improved separation efficiency of the charge carriers. Furthermore, the BiOI/PAER composites exhibited excellent cyclic utilization stability, which is a key factor for their potential practical applications.Polysaccharides are known to modify binding of proteins at interfaces and this paper describes studies of these interactions and how they are modified by pH. Specifically, the adsorption of human serum albumin on to polystyrene latex and to silica is described, focusing on how this is affected by hyaluronan. Experiments were designed to test how such binding might be modified under relevant physiological conditions. Changes in adsorption of albumin alone and the co-adsorption of albumin and hyaluronan are driven by electrostatic interactions. Multilayer binding is found to be regulated by the pH of the solution and the molecular mass and concentration of hyaluronan. Highest adsorption was observed at pH below 4.8 and for low molecular mass hyaluronan (≤150 kDa) at concentrations above 2 mg ml<sup>−1</sup>. On silica with grafted hyaluronan, albumin absorption is reversed by changes in solvent pH due to their strong electrostatic attraction. Albumin physisorbed on silica surfaces is also rinsed away with dilute hyaluronan solution at pH 4.8. The results demonstrate that the protein adsorption can be controlled both by changes of pH and by interaction with other biological macromolecules.A highly sensitive o-phenylenediamine (OPD) sensor based on a Fe3O4 doped with functionalized multi-walled carbon nanotubes (Fe3O4@F-MWCNTs) composite fabricated glassy carbon electrode (GCE) was developed. The modified Fe3O4@F-MWCNTs/GCE showed an enhanced current (ipa) response toward OPD relative to that of a Fe3O4/GCE, F-MWCNTs/GCE, and a bare GCE. Under optimum conditions, the Fe3O4@F-MWCNTs/GCE showed a wide linear range remove at OPD concentrations of 0.6–80 µM. The limit of detection and sensitivity of the F-MWCNTs/GCE, Fe3O4/GCE sensor were found to be 50 µM, and 2.8002 mA mM<sup>−1</sup> cm<sup>−2</sup>, respectively. The developed sensor showed excellent accumulation time, good repeatability, and operational stability. The obtained results suggest that the development of composite could be an effective electro-catalyst and it can play a vital role in biomedical, pharmaceutical, and hazardous free environmental applications. In order to modify the self-assembly of sucrose esters (SEs) in sunflower oil, we used sunflower lecithin (SFL) as co-surfactant. It is hypothesized that SFL modifies the self-assembly of SEs by interrupting the extensive hydrogen bonding between SEs monomers.

The addition of SFL into SEs induced gelation of the mixed surfactant system oleogels at all studied ratios. The 7:3 SEs:SFL combination showed enhanced rheological properties compared to the other studied ratios, which suggests better molecular ordering induced by SFL. The modifications might have been caused by interference in the hydrogen bonding, connecting the polar heads of SEs molecules in the presence of SFL. This effect was confirmed by thermal behavior and small angle X-ray diffraction (SAXD) analysis.



From the crystallization and melting analyses, it was shown that the peak temperature, shape and enthalpy decreased as the SFL ratio increases. Meanwhile, the bi-component oleogels exhibited new peaks in the SAXD profile, which imply a self-assembly modification. The microscopic study through polarized and electrons revealed a change in the structure. Therefore, it can be concluded that a synergistic effect between SEs and SFL, more particularly at 7:3 ratio, towards sunflower oil structuring could be obtained. These findings shed light for greater applications of SEs as structuring and carrier agent in foods and pharmaceutical.High-order (higher-than 2nd-order) gas-kinetic schemes for solving the Navier-Stokes equations have been studied in recent years. In addition to the use of high-order reconstruction techniques, many terms are used in the Taylor expansion of the equilibrium and non-equilibrium gas distribution functions in the high-order gas kinetic flux function. Therefore, a large number of coefficients need to be determined in the calculation of the time evolution of the gas distribution function at cell interfaces. As a consequence, the high-order flux function takes much more computational time than that of a 2nd-order gas-kinetic scheme. This paper aims to simplify the evolution model by two steps. Firstly, the coefficients related to the 2nd-order spatial and temporal derivatives of a distribution function are redefined to reduce the computational cost. Secondly, based on the physical analysis, some terms can be removed without loss of accuracy. As a result, through the simplifications, the computational efficiency of the high-order scheme is increased significantly. In addition, a self-adaptive numerical viscosity is designed to minimize the necessary numerical dissipation. Several numerical examples are tested to demonstrate the accuracy and robustness of the current scheme.View full text Amorphous Polymer Tg(°C) Poly(chlorotrifluoroethylene) 87 Poly(vinyl chloride), PVC 83 Poly(vinyl fluoride), PVF 52 Poly(vinylidene chloride), PVDC -17 Poly(vinylidene fluoride), PVDF -34 Teflon, PTFE 119 Polychloroprene, Neoprene -36 Poly(acrylamide) 165 Poly(N,N-dimethylacrylamide) 106 Poly(2-cyanobutyl acrylate) 111 Poly(2-cyanoethyl acrylate) 4 Poly(2-ethylhexyl acrylate) -53 Poly(2,2,3,3-tetrafluoropropyl acrylate) -24 Poly(3,3,5-trimethylcyclohexyl acrylate) 29 Poly(4-cyanobutyl acrylate) -38 Poly(acrylic acid), PAA 101 Poly(benzyl acrylate) 4 Poly(butyl acrylate) -53 Poly(cyanomethyl acrylate) 23 Poly(cyclohexyl acrylate) 15 Poly(dodecyl acrylate) -19 Poly(ethyl acrylate) -23 Poly(hexyl acrylate) -59 Poly(isobornyl acrylate) 86 Poly(isobutyl acrylate) -34 Poly(isopropyl acrylate) -2 Poly(methyl acrylate), PMA 10 Poly(nonyl acrylate) -74 Poly(octadecyl acrylate) 40 Poly(phenoxyethyl acrylate) 6 Poly(propyl acrylate) -42 Poly(sec-butyl acrylate) -21 Poly(tert-butyl acrylate) 38 Poly(tetrahydro furfuryl acrylate) -14 Poly(1-butene) -29 Poly(1-octene) -55 Poly(1-pentene) -35 Poly(4-methylpent-1-ene) 29 Poly(cyclohexylthene) 120 Poly(ethylene) -80 Poly(isobutene) -70 Poly(propylene) -10 Poly(1-(tert-butyl)ethene) 64 Poly(heptane-1,7-diyl teraphthalamide) 116 Poly(8-aminooctanoic acid), Nylon 8 50 Poly(caprolactam), Nylon 6 51 Poly(hexamethylene sebacamide), Nylon 6,10 46 Poly(hexamethylene sebacamide), Nylon 6,10 46 Poly(iminoadipoyliminohexamethylene), Nylon 7,6 52 Poly(iminosebacoyliminododecamethylene), Nylon 10,10 53 Poly(m-phenylene terephthalamide), Nomex MPDI 264 Poly(p-phenylene terephthalamide), Kevlar, PPTA 327 Poly(ω-dodecanamide), Nylon 12 40 Poly(ω-undecanamide), Nylon 11 44 Poly(4,4'-methylenedioxy dibenzoic anhydride) 134 Poly(4,4'-pentamethylenedibenzoic anhydride) 47 Poly(4,4'-tetramethylenedibenzoic anhydride) 43 Poly(isophthalic anhydride) 112 Poly(1,2-ethylene carbonate) 17 Poly(1,2-propylene carbonate) , PPC 37 Poly(1,4-cyclohexanecarbonate) 127 Poly(1,5-pentylene carbonate) 4 Poly(1,6-hexylene carbonate) -2 Poly(1,8-octylene carbonate) -8 Poly(2,6,3',5'-tetrachloro bisphenol A carbonate) 227 Poly(3,3'-oxydiphenylene carbonate) 90 Poly(4,4'-thiodiphenylene carbonate) 118 Poly(Bisphenol A carbonate) 150 Poly(Bisphenol AP carbonate) 187 Poly(Bisphenol B carbonate) 141 Poly(Bisphenol C carbonate) 108 Poly(tetramethyl Bisphenol A carbonate) 193 Poly(Bisphenol E carbonate) 142 Poly(Bisphenol F carbonate) 134 Poly(methyl cyanoacrylate) 162 Poly(ethyl cyanoacrylate) 149 Poly(butyl cyanoacrylate) 106 Poly(1,2-butadiene) -13 Poly(1-pentenyene) -96 Poly(1,4-butadiene) -105 Poly(1-methyl-1-butenylene) -70 Poly(norbornene) 43 Poly(1,4-butylene adipate) -68 Poly(2-ethyl-2-methylpropylene terephthalate) 55 Poly(1,4-butane sebacate) -60 Poly(caprolactone) -66 Poly(decamethylene terephthalate) 10 Poly(nonamethylene terephthalate) 16 Poly(ethylene 2,6-naphthalate) 119 Poly(ethylene adipate) 44 Poly(ethylene phthalate) 24 Poly(ethylene terephthalate) 72 Poly(hexamethylene terephthalate) 18 Poly(neopentyl glycol succinate) -17 Poly(RV-3-hydroxybutyrate 0 Poly(trimethylene terephthalate) 55 Poly(tetramethylene isophthalate) 24 Poly(tetramethylene terephthalate) 40 Poly(Bisphenol A terephthalate) 112 Poly(tetramethyl bisphenol A terephthalate) 218 Poly(tetrachloro Bisphenol A terephthalate) 210 Poly(diisopropyl Bisphenol A terephthalate) 135 Poly(diisobutyl Bisphenol A terephthalate) 100 Poly(Bisphenol C terephthalate) 171 Poly(bisphenol AP isophthalate) 200 Polyglycolide, PGL 39 Poly(lactic acid), PLA 59 Poly(ether ketone ketone), PEEK 164 Poly(4,4'-dichlorobenzophenone), PEK 155 Poly(hydroquinone)-alt-(4,4'-dichlorobenzophenone)], PEEK 146 Poly(hydroquinone-alt-[1,4-bis(4-fluorobenzoyl)benzene]), PEEKK 159 Poly(diethyl fumarate) 10 Poly(dimethyl fumarate) -14 Poly(3-hexoxypropylene oxide) -84 Poly(1-chloromethyl)ethylene oxide) -24 Poly(epichlorohydrin) -22 Poly(ethylene glycol), PEG -67 Poly(propylene glycol), PPG -74 Poly(tetrahydrofuran), PTHF, PTMG -86 Poly(trimethylene glycol) -77 Polyacetal, Poly(methylene oxide), POM -66 Poly(dimethyl itaconate), PDMI 99 Poly(di(n-propyl) itaconate) 32 Poly(ethyleneketone), PEK 15 poly(prop-1-ene)-alt-(carbon monooxide)] 38 Poly(1-(Diethylamino)ethyl methacrylate) 20 Poly(1-(Dimethylamino)ethyl methacrylate) 18 Poly(2-hydroxyethyl methacrylate), PHEMA 77 Poly(2-hydroxypropyl methacrylate) 72 Poly(2-phenylethyl methacrylate) 26 Poly(2,2,2-trifluoroethyl methacrylate) 74 Poly(2,2,3,3-tetrafluoropropyl methacrylate) 71 Poly(4-tert-butylcyclohexyl methacrylate) 130 Poly(benzyl methacrylate) 55 Poly(butyl methacrylate) 20 Poly(cyclohexyl methacrylate) 116 Poly(decyl methacrylate) -63 Poly(dodecyl methacrylate) -55 Poly(ethyl methacrylate), PEMA 65 Poly(glycidyl methacrylate) 61 Poly(hexadecyl methacrylate) 16 Poly(hexyl methacrylate) -5 Poly(isobornyl methacrylate) 110 Poly(isobutyl methacrylate) 57 Poly(isodecyl methacrylate) -41 Poly(isopropyl methacrylate) 83 Poly(methacrylic acid), PMAA 228 Poly(methyl methacrylate), PMMA 105 Poly(neopentyl methacrylate) 26 Poly(octadecyl methacrylate) 38 Poly(octyl methacrylate) -45 Poly(pentyl methacrylate) 2 Poly(phenyl methacrylate) 110 Poly(propyl methacrylate) 42 Poly(tert-butyl methacrylate) 115 Poly(tetradecyl methacrylate) 9 Poly(tetrahydrofurfuryl methacrylate) 53 Poly(acrylonitrile), PAN 109 Poly(methacrylonitrile) 115 Poly(2-chloro-p-xylene) 83 Poly(p-phenylene), PPP 265 Poly(p-xylene) 70 Poly(1,4-phenyl ether), PPE 87 Poly(2,6-dimethyl-p-phenylene oxide), PPO 214 Poly(2,6-diphenyl-p-phenylene oxide) 224 Poly(2-methoxystyrene) 75 Poly(2-methylstyrene) 136 Poly(3-methylstyrene) 97 Poly(4-ethylstyrene) 52 Poly(4-isopropylstyrene) 87 Poly(4-methoxy-2-methylstyrene) 87 Poly(4-methoxystyrene) 113 Poly(4-methylstyrene) 104 Poly(4-phenylstyrene) 149 Poly(4-tert-butylstyrene) 129 Poly(α-methylstyrene), PaMS 172 Polystyrene, PS 100 Poly(2-chlorostyrene) 122 Poly(4-bromostyrene) 138 Poly(4-chlorostyrene) 125 Poly(4-fluorostyrene) 103 Poly(1,4-biphenyl ether ether sulfone), PPSU 209 Poly(1,4-phenylene ether ether sulfone), PEE 206 Poly(1,4-phenylene ether-sulfone), PES 217 Poly(bisphenol S-alt-terephthalic acid) 246 Poly{[bis(4-chlorophenyl)sulfone]-alt-[bisphenol-A]}, PSU 183 Poly(1,4-phenylene sulfide), PPS 90 Poly(ethylene sulfide) -50 Poly(propylene sulfide), PPS -46 Poly[(1,4-butanediol)-alt-(1,6-hexamethylene diisocyanate)], PTMG -HMDI 22 Poly[(diethylene glycol)-alt-(1,6-hexamethylene diisocyanate)], PEG 100 -HMDI 8 Poly[(ethylene glycol)-alt-(hexamethylene diisocyanate)],PEG 50 -HMDI 27 Poly[(butane-1,4-diol)-alt-[bis(4-isocyanatophenyl)methane]], Butane-1,4-diol -MDI 89 Poly[(ethylene glycol)-alt-[bis(4-isocyanatophenyl)methane]], EG 50 -MDI 139 Poly(vinyl alcohol), PVOH, PVA 80 Poly(4-hydroxystyrene), PVAc, PVA 157 Poly(vinyl acetate), PVAc, PVA 33 Poly(vinyl benzoate) 71 Poly(vinyl butyrate), PVB 5 Poly(vinyl formate) 34 Poly(vinyl propionate) 10 Poly(vinyl stearate) 45 Poly(butyl vinyl ether) -54 Poly(ethyl vinyl ether) -41 Poly(hexyl vinyl ether) -76 Poly(isobutyl vinyl ether) -19 Poly(isopropyl vinyl ether) -3 Poly(methyl vinyl ether) -28 Poly(octyl vinyl ether) -80 Poly(propyl vinyl ether) -49 Poly(trifluoromethoxy 1,1-difluoroethylene) -5 Poly(vinyl butylal) 70 Poly(4-chlorophenyl vinyl ketone) 63 Poly(methyl isopropenyl ketone) 97 Poly(phenyl vinyl ketone) 49 Poly(vinyl ethyl ketone) -60 Poly(vinyl methyl ketone) 28 Poly(butyl vinyl thioether) -20 Poly(ethyl vinyl thioether) -7 Poly(methyl vinyl thioether) -1 Poly(vinyl phenyl sulfide) 113 1The Tgs are the average of one or more experimental values.